

Optimization of a three-row air-suction *Brassica chinensis* precision metering device based on CFD-DEM coupling simulation

Xinping Sun^{1,2}, Hua Li^{2,3*}, Xindan Qi¹, Dinghao Feng^{1,2}, Jianqi Zhou^{2,3}, Yongjian Wang^{2,3}, Samuel Mbugua Nyambura^{2,3}, Xiaoyu Zhang⁴, Xi Chen^{1,2}

(1. College of Mechanical and Power Engineering, Nanjing Tech University, Nanjing 211816, China;

2. Key Laboratory of Intelligent Agricultural Equipment in Jiangsu Province, Nanjing Agricultural University, Nanjing 210031, China;

3. College of Engineering, Nanjing Agricultural University, Nanjing 210031, China;

4. Jiangsu Xuzhou Transportation Planning and Design Institute, Xuzhou 221000, China)

Abstract: This study aimed to optimize a three-row air-suction *Brassica chinensis* precision metering device to improve the low seeding performance. ANSYS 17.0 Software was used to analyze the effect of different numbers of suction holes and different suction hole structures on the airflow field. It was found that a suction hole number of 60 was beneficial to the flow field stability and a conical hole structure was beneficial to the adsorption of seeds. Box-Behnken design experiments were carried out with negative pressure, rotational speed, and hole diameter as the experimental factors. The optimal parameter combination was achieved when the negative pressure was 3.96 kPa, the rotational speed of the seeding plate was 1.49 rad/s and the hole diameter was 1.10 mm. The qualification rate of inner, middle, and outer rings were 87.580%, 90.548%, and 90.117%, respectively, and the miss seeding rate of inner, middle, and outer rings were 10.915%, 7.139%, and 5.920%, respectively.

Keywords: *Brassica chinensis*, metering device, airflow field, Box-Behnken design

DOI: 10.25165/ijabe.20231603.7812

Citation: Sun X P, Li H, Qi X D, Feng D H, Zhou J Q, Wang Y J, et al. Optimization of a three-row air-suction *Brassica chinensis* precision metering device based on CFD-DEM coupling simulation. Int J Agric & Biol Eng, 2023; 16(3): 130–142.

1 Introduction

Vegetables are essential in the daily lives of people all over the world because they provide essential vitamins, minerals, and other nutrients to the body^[1]. *Brassica chinensis*, also known as Chinese cabbage, is a species of *Brassica* in the cruciferous family. It has a short growth cycle, strong resistance to adversity, a wide range of adaptation, and rich nutritional value. It is the most abundant crop in China in terms of cultivation area and total production and is also considered an important crop in temperate, subtropical, and tropical regions of the world^[2,3]. With the continuous expansion of planting area, it is necessary to study the mechanized precision sowing technology of *Brassica chinensis*. The metering device, as the core component of the precision seeder, has a direct impact on the final operation effect of the seeder. There are two main types of metering devices, mechanical and pneumatic, but pneumatic metering devices are more widely used because of their high accuracy, less damage to

the seed, and suitability for high speeds^[4].

The pneumatic metering devices mainly adsorb seeds through the negative pressure chamber created by the fan, which needs to be sealed and evenly distributed during the working process^[5]. The faster the seeding plate rotates during the sowing of *Brassica chinensis*, the less time the metering device has to fill, which can easily lead to missed rate and a low qualified rate. The performance of the air-absorbing metering device is mainly influenced by negative pressure, the rotation speed of the seeding plate, the number of suction holes, and the shape of the air chamber^[6]. Due to the complex movement of the seeds during the actual operation of the metering device, it is not possible to visually observe the effect of the seeds on the airflow field. Therefore, it is necessary to use particle simulation, fluid simulation, and two-way coupling methods to explore the interaction between seeds and airflow fields^[7].

In recent years, Discrete Element Method (DEM) and Computational Fluid Dynamics (CFD) simulation have been widely used in industry and agriculture to solve the problems encountered in observing the complex movements of machines^[8,9]. DEM is generally considered to have been introduced by Cundall in 1979 as a numerical method for displaying solutions. DEM discrete unit method is a numerical calculation method for analyzing the dynamics of material systems after FEM and CFD. DEM performs updating of particle position and velocity by building a parametric model of the solid particle system^[10,11]. The use of coupling CFD-DEM for the study of seed dispensers is becoming increasingly popular among researchers. Liu et al.^[12] used CFD-DEM simulations to investigate the fluid dynamics of a thin rectangular fluidized bed as the pressure increases from 1 bar to 10 bar, showing that the bubble size and pressure fluctuations decrease as the pressure increases. Taghinezhad, Jafari, and Alimardani^[13] designed a new

Received date: 2022-07-19 **Accepted date:** 2023-05-15

Biographies: Xinping Sun, MS candidate, research interest: accurate planting, Email: xinpingsun2022@163.com; Xindan Qi, MS, Associate Professor, research interest: accurate planting and harvesting, Email: xindanqi@njtech.edu.cn; Dinghao Feng, MS candidate, research interest: accurate planting, Email: dinghaofeng@njtech.edu.cn; Jianqi Zhou, MS candidate, research interest: accurate planting, Email: njauzjq@163.com; Yongjian Wang, PhD, Associate Professor, research interest: accurate planting and harvesting, Email: yjwang@njau.edu.cn; Samuel Mbugua Nyambura, PhD candidate, research interest: technology and equipment of biomass conversion, Email: accessmbugua@gmail.com; Xiaoyu Zhang, MS candidate, research interest: accurate planting, Email: 2921367620@qq.com; Xi Chen, MS candidate, research interest: accurate planting, Email: njut_chenxi@163.com.

*Corresponding author: Hua Li, PhD, Professor, research interest: accurate planting and harvesting. College of Engineering, Nanjing Agricultural University, Nanjing 210031, China. Tel: +86-13951740692, Email: lihua@njau.edu.cn.

sugar cane metering device and found the best combination of operating parameters by studying the effects of the metering device tooth length and the speed of the sugar cane blank metering device. The results showed that a metering device with a 2 cm tooth length and a forward speed of 0.75 m/s was the best combination for the sugar cane blank metering device and the consistency ratio was calculated to be less than 0.1, indicating that the results were acceptable. Lei et al.^[14] conducted a numerical study of air-solid flow in a seed-feeding device of an air-assisted centralized metering system by coupling the discrete element method (DEM) and computational fluid dynamics (CFD) to investigate and analyze the effects of the throat area, throat length, airflow inlet velocity, and seed feed rate on the air field and seed motion. The results show that throat area and airflow inlet velocity mainly affect the airflow exit velocity and the seed velocity in the airflow direction, which is caused by drag, while the seed motion is slightly affected by throat length and seed feed rate. This demonstrates the reliability of the coupled DEM-CFD method as a tool for understanding the physical phenomena of seed movement in the airflow field^[15,16]. Zhang et al.^[17] designed the roller for seeds of different sizes, a variable-size pneumatic cylinder precision seed-metering device, which could realize the precision seeding of different diameter seeds without changing the roller. Analyzed the effect of inlet tube size and eyelet shape on airflow velocity using basic principles of ANSYS fluid simulation.

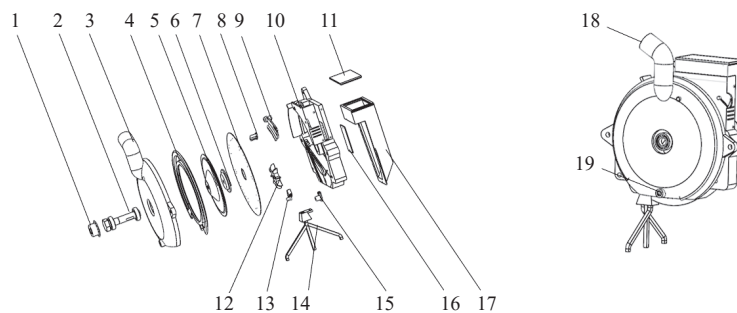
This study aimed to optimize a three-row air-suction *Brassica chinensis* precision metering device to improve seeding efficiency. Discrete Element Method (DEM) and Computational Fluid Dynamics (CFD) were used to simulate the operation of a three-row air-suction *Brassica chinensis* precision metering device. The influence of the number and structure of suction holes on the

airflow velocity and pressure in the negative pressure chamber was analyzed through ANSYS fluid simulation. A quadratic rotation orthogonal combination of negative pressure, the rotational speed of the seeding plate, and the suction hole diameter were used as experimental factors to investigate the seeding performance of the metering device. This study uses ANSYS finite element and EDEM joint simulation to greatly reduce the cost of research and development, while this design product can improve the efficiency of *Brassica chinensis* mechanical planting and provide a theoretical basis for other one-tool multi-row planting machines.

2 Materials and methods

2.1 Structure and working principle of the metering device

A three-row air-suction *Brassica chinensis* precision metering device belongs to agricultural machinery, the metering device mechanism mainly left casing, three-row seeding plate, lower seed clearing mechanism, super clearing mechanism, seed meter base, seed tube, and seed box, as shown in Figure 1. This metering device adopted a nylon sealing ring and three rows of seed seeding plates to ensure the stability of the entire negative pressure air chamber. The seed layer height control board adjusted the height of *Brassica chinensis* seeds piled in the seed filling area to reduce the mutual friction between the seeds, which was conducive to the adsorption of the seeds by the suction holes, and the seed stirring wheel increased the fluidity of the seeds in the seed filling area to assist the seed filling. After the suction hole absorbed the seeds, the seeds passed through the seed cleaning area, and the excess seeds in the hole were removed under the action of the seed cleaning mechanism to reduce the reseeding rate. Then the seeds reached the seeding area and lost the negative pressure instantly, and fell into the seed tube under the action of gravity.



1. Sprocket 2. Rotating shaft 3. Left casing 4. Sealing ring 5. Inner cover 6. Outer cover 7. Three-row seeding plate 8. Lower seed clearing mechanism 9. Upper clearing mechanism 10. Seed meter base 11. Seedbox cover 12. Seed stirring wheel 13. Rotating parts 14. Seed tube 15. Seed stirring wheel bracket 16. Seed layer height baffle 17. Seed box 18. Negative pressure outlet 19. Positive pressure inlet.

Figure 1 A three-row air-suction *Brassica chinensis* precision metering device

2.2 Determination of the main parameters of metering device

According to Agricultural Machinery Design Manual^[18], the diameter of the seeding plate was between 80-240 mm, and the center linear velocity (V_c) of the suction hole was not more than 0.35 m/s. It was calculated that the rotational speed of the seeding plate was less than or equal to 4.375 rad/s. The plant spacing (L) of *Brassica chinensis* seeds was 40-50 mm, and the row spacing (P) was about 100 mm. The schematic diagram of *Brassica chinensis* planting is shown in Figure 2. To investigate the correlation between the diameter (D) of the seeding plate and the seed-filling time (T), the equation for calculating was as follows:

$$T = \frac{S}{V_c} \tag{1}$$

$$S = \frac{\alpha\pi}{180} \left(\frac{D}{2} - d_c \right) \tag{2}$$

$$V_c = \frac{n\pi}{30} \left(\frac{D}{2} - d_c \right) \tag{3}$$

$$Z = \frac{60V_m}{nl} \tag{4}$$

where, T is the seed-filling time, s; S is the arc length of the seed-filling zone, m; V_c is the center linear speed of the suction hole, m/s; α is the angle of the seed-filling zone, ($^\circ$); D is the diameter of the seeding plate, m; d_c is the distance from the center of the suction hole to the edge of the seeding plate, m; n is the rotational speed of the seeding plate, r/min; Z is the number of suction holes; V_m is the speed of the planter, m/s; l is the plant spacing of the seeds, mm. It

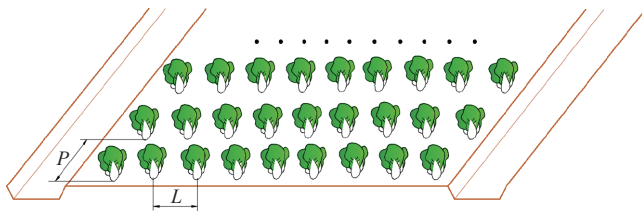


Figure 2 Schematic diagram of *Brassica chinensis* planting

was summarized by Equations (1)-(4):

$$T = \frac{\alpha}{6n} \tag{5}$$

The planter was called high-speed seeding when its forward speed was greater than 6 km/h and less than 18 km/h. Therefore, the number of suction holes on the seeding plate was calculated by Equation (4) and the known data of the previous was $48 \leq Z \leq 144$ ^[19]. From Equation (5), the seed-filling time T was determined by the angle of the seed-filling zone and the rotational speed of the seeding plate, which was not directly related to the value of the diameter of the seeding plate. The range of triaxial dimensions was measured several times using a Vernier caliper, and the measurements are listed in Table 1. The diameter of the suction hole was determined according to Equation (6), and the range of d was calculated to be 1.07-1.11 mm.

$$d = (0.64 - 0.66)W \tag{6}$$

Table 1 Measured dimensions of *Brassica chinensis* seeds

Parameter	Range	Mean	Standard error
Length/mm	1.37-2.28	1.82	0.15
Width/mm	1.33-1.91	1.68	0.13
Thickness/mm	1.32-1.98	1.66	0.16
Thousand seed mass/g	2.39-2.43	2.41	0.013

2.3 Determination of the number and structure of suction holes in the seeding plate

2.3.1 Determination of the number of suction holes

When sowing seeds in an air-suction metering device, the

number of holes had a significant effect on the airflow field of the metering device, so it was necessary to carry out a simulation study to determine the optimal number of holes in the seeding plate for sowing *Brassica chinensis* seeds. According to the calculation formula for the design of the holes, it can be concluded that the number of holes on the seeding plate ranged from more than 48 to less than 144. When designing the number of suction holes, the spacing between the suction holes was considered to avoid head-to-tail contact between seeds and interfering with the working performance of the metering device. The calculation of the distance between adjacent suction holes is shown in Equation (7). S_E was 1.72 mm, $S_L \geq 6.28$ mm, and $Z \leq 110$. Combining the above calculations, the number of suction holes was determined to range from 48 to 110.

$$\begin{cases} S_E = \sqrt[3]{L\bar{W}\bar{H}} \\ S_L \geq S_E + 2L_{MAX} \\ S_L = \frac{\pi D}{Z} \end{cases} \tag{7}$$

where, S_E is the average equivalent diameter, mm; \bar{L} is the average length of the seeds, mm; \bar{W} is the average width of the seeds, mm; \bar{H} is the average thickness of the seeds, in mm; S_L is distance between adjacent suction holes, mm; L_{MAX} is maximum of seeds length, mm.

Based on previous results from laboratory studies, the larger the number of holes on the seeding plate, the greater the wind pressure consumed^[20]. The lower number of suction holes, in turn affects the seeding efficiency of *Brassica chinensis*. Comprehensive consideration of the agronomic requirements, processing costs, and fan consumption, the seeding plates with the number of suction holes of 60, 75, and 90 were selected for study comparison in this study^[20,21]. To further determine the optimal number of holes in the seeding plate, it was necessary to simulate the number of different holes on the seeding plate. The pressure cloud diagram and airflow vector diagram of the simulation results are shown in Figures 3 and 4.

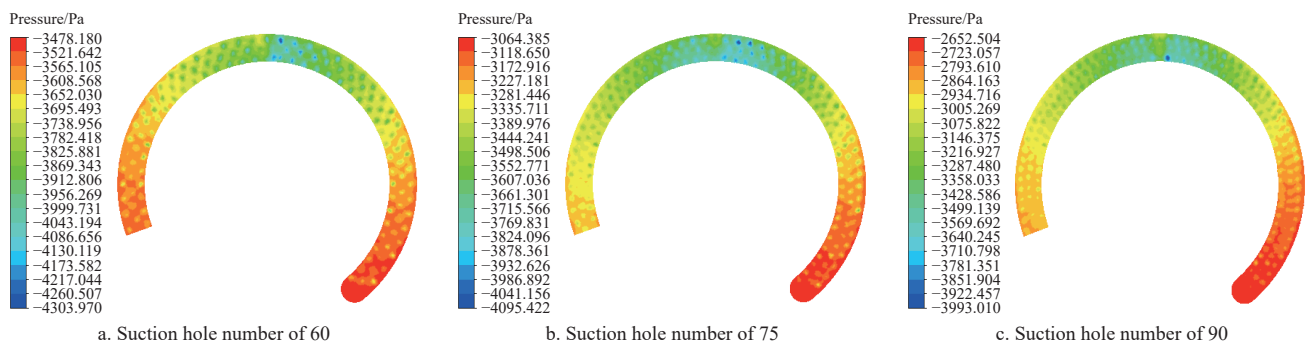


Figure 3 Pressure cloud diagram of negative pressure chamber with different hole numbers

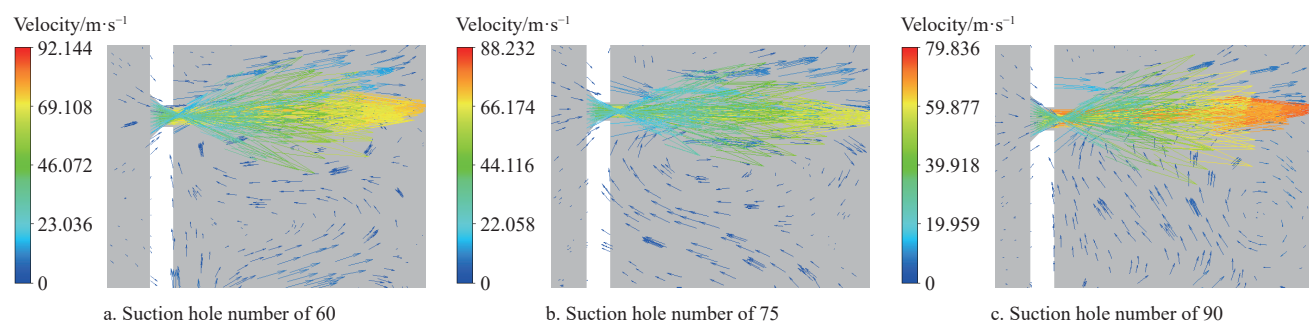


Figure 4 Vector diagram of the airflow velocity of a suction hole with different hole numbers

Figure 3 shows the overall pressure cloud diagrams of the three kinds of seeding plates with different numbers of holes that were similar, and they all decreased from the middle to the two sides. The pressure range of the seeding plate with 60 holes was $(-4.304-3.478)$ kPa, the pressure range of the seeding plate with 75 holes was $(-4.095-3.064)$ kPa and the pressure range of the seeding plate with 90 holes was $(-3.993-2.653)$ kPa. As the number of holes increased, the pressure field value became small. Properly reducing the number of holes on the seeding plate improved the stability of the flow field and was conducive to seed filling. Figure 4 shows that the more the number of holes, the smaller the velocity around the suction holes, and the less disturbance of the airflow field to the suction holes on the seeding plate with 60 holes, which was beneficial to the overall stability of the flow field and the reliability of the suction holes for seed adsorption.

According to the simulation analysis of the airflow field in Figures 3 and 4, it can be concluded that the selection of the seeding plate with the number of holes 60 was conducive to the stability of the flow field, and the smaller the number of suction holes, the loss of negative pressure was reduced.

2.3.2 Determination of the structure of the suction holes

The shape of the hole in the seeding plate is one of the important conditions to ensure that *Brassica chinensis* seeds can be effectively adsorbed by the hole. A large number of scholars have studied the shape of the seeding plate. Among them, Yin et al.^[22] designed and tested the suction nozzle type holes of pneumatic-sheave combined vegetable precision seed metering device, and designed a variety of suction nozzle type holes such as straight, conical, cylindrical, and waist round holes according to the size of the three axes of vegetable seeds. The experimental results showed that the suitable nozzle types for *Brassica chinensis*, carrot, and aubergine were: conical hole, round waist hole, and straight hole respectively. The seed releasing rate was 97.0%, 95.4%, and 93.7%

under the optimum vacuum and speed conditions respectively, meeting the sowing requirements. Fallak evaluated seven vacuum nozzles in a stationary device similar to horticultural seed flat seeders. The results showed that nozzles with an entrance cone were the least sensitive to changes in pickup height, while pointed nozzles were the most sensitive. The smallest section of the nozzle should be as wide as possible in order to reduce pressure^[23]. Four different shapes of holes were selected for airflow simulation to investigate the effect of different shapes of holes on the pressure and velocity of the suction surface. The suction hole shape is shown in Figure 5.

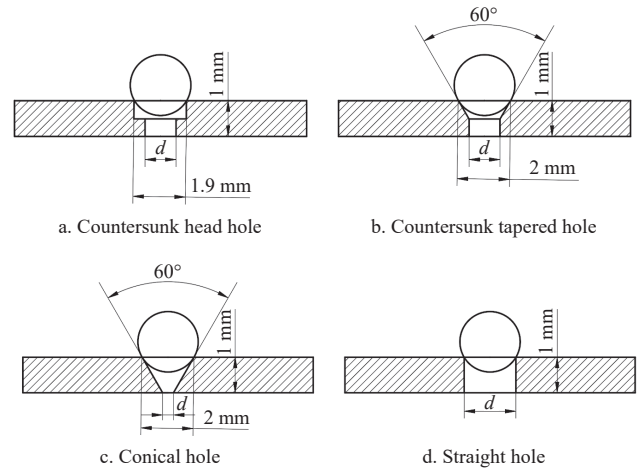


Figure 5 Schematic diagram of the suction hole structure

The metering device was meshed and simulated. The inlet pressure was set to 0 kPa, the outlet pressure was set to -5 kPa, and the number of iteration steps was set to 1500 steps. The negative pressure and velocity clouds for different suction hole shapes are shown in Figures 6-9.

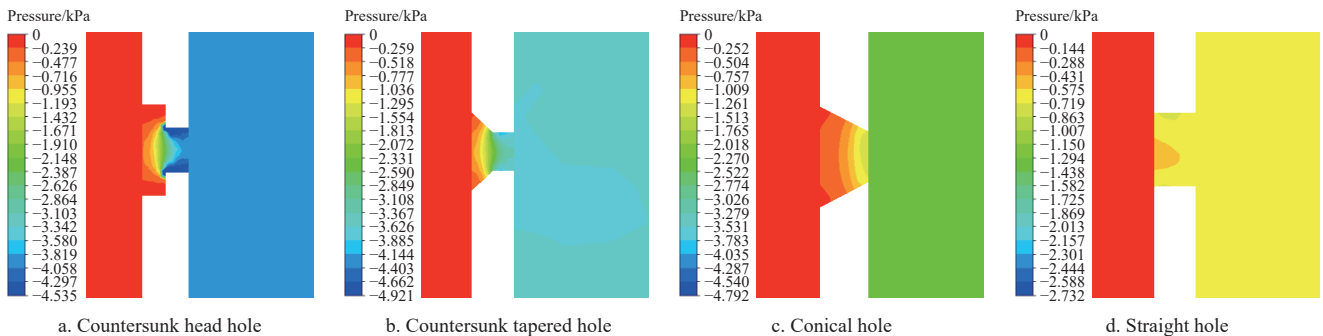


Figure 6 Axial pressure cloud diagram of different types of holes

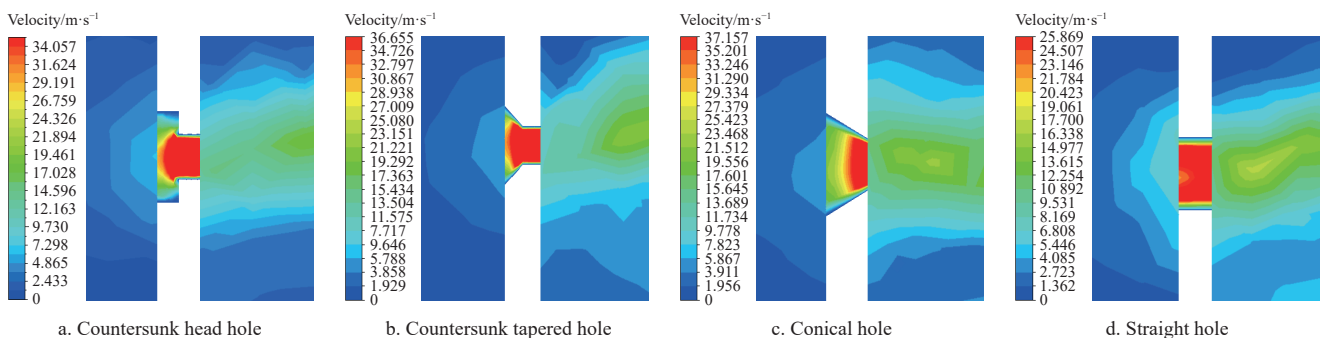


Figure 7 Axial velocity cloud diagram of different types of holes

Figure 6 shows that the axial pressure cloud diagrams of the suction holes under different shapes were different and the airflow

layer in the positive and negative pressure areas had little change. Figure 6a shows the pressure cloud diagram of the countersunk

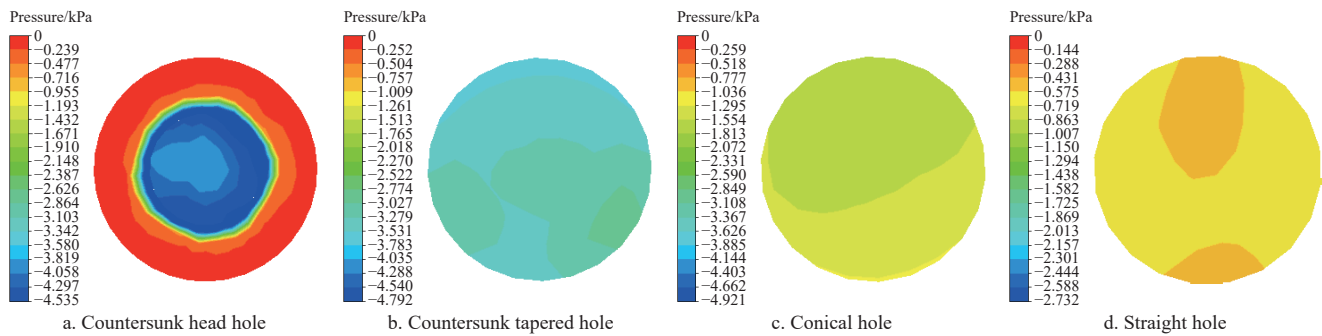


Figure 8 Enlarged pressure cloud diagram at seed suction surface of different types of holes

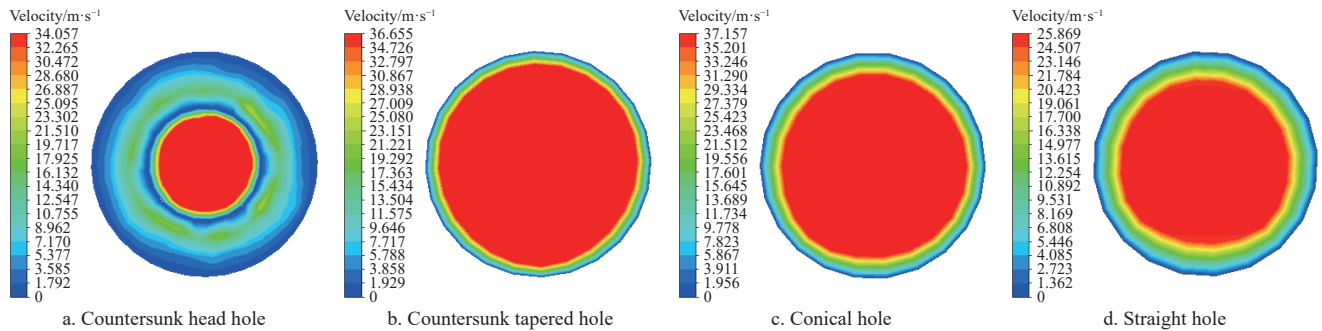


Figure 9 Enlarged velocity cloud diagram at seed suction surface of different types of holes

head. The overall pressure of the countersunk head was relatively small, while the pressure of the straight pipe part of the countersunk head hole was relatively large, and the largest point was mainly concentrated on the inner wall of the countersunk head hole. There was a small change in the airflow layer of the countersunk taper hole, and the pressure of the straight pipe part of the countersunk taper hole was basically the same as that in the negative pressure area, and the pressure value was about -3.630 to 3.278 kPa, while the pressure variation in the tapered section was similar to that in the countersunk section of the countersunk hole. The pressure distribution of the conical hole decreased annularly from the positive pressure area to the negative pressure area, and the pressure near the edge of the negative pressure area was about -1.500 kPa. The pressure change at the square hole was small, and the pressure value was concentrated around -0.750 kPa as a whole.

Figure 7 shows that the axial velocity of different hole shapes was larger on the side connected to the negative pressure area, which formed a nearly hemispherical velocity distribution in the air layer. The airflow velocity in most areas in the center of the hole was relatively large, while the velocity near the wall approached 0. As can be seen from Figure 8, the pressure distribution of the suction surfaces of different shapes was uneven, the pressure value in the middle part was larger, and the pressure value around the surface was smaller. The pressure at the suction surface was arranged in order from large to small as the countersunk head hole, countersunk taper hole, conical hole, and straight hole. Figure 9 shows that different shapes of holes had a significant impact on the speed of the seed suction surface. The speed distribution of the seed suction surface was relatively uniform. The center of the hole was the highest distribution concentration area, and the inner wall of the hole had a lower speed. The speed at the suction surface was arranged in order from large to small as the conical hole, countersunk taper hole, countersunk head hole, and straight hole.

Through simulation analysis of the velocity and pressure of the airflow field, while considering the simplicity and rationality of the

hole structure, the conical hole was selected as the suction hole on the seeding plate, and the pressure distribution on the conical hole met the requirements of the suction hole for adsorbing seeds.

2.4 Working process of the metering device

Hu et al.^[24] used the CFD-DEM coupling simulation method to observe the distribution characteristics of rapeseed seeds in an air-assisted centralized seed-metering device to optimize parameters. To verify the reasonableness of the airflow field simulation, this paper investigated the seeding performance under different conditions of the seed dispenser simulation by changing the diameter of the suction hole. During the simulation process, the number of seeds in the suction holes was observed by the naked eye. Since the coupling CFD-DEM simulation required a lot of computer resources, it took about 90 h for just 1500 seeds, so the number of seeds observed in this simulation was 60. The simulation process is shown in Figure 10. The qualification rate and miss-seeding rate were calculated from the data counted in each group according to Chinese standard GB/T6973-2005 - Testing Methods of Single Seed (Precision Drills), as listed in Table 2.

As can be seen from Table 2, for the same hole diameter, the middle ring had a higher qualification rate compared to the inner and outer rings. The qualification rate was generally low for hole diameters of 0.8 mm and the high rate of miss-seeding seeds was probably because smaller holes required a larger negative pressure to adsorb the seeds. For a hole diameter of 1.0 mm, the metering device performed better, with a qualification rate above 91% and a miss-seeding rate below 9%. For a hole diameter of 1.2 mm, the seeding performance of the metering device was optimal. The CFD-DEM coupling simulation provided a reference for the metering device performance test. However, the vibration problem of the metering device was ignored, and the validity of the coupling simulation needs to be verified later.

2.5 Performance parameter optimization of metering device

2.5.1 Test materials and equipment

The test material selected in this study was the seeds of

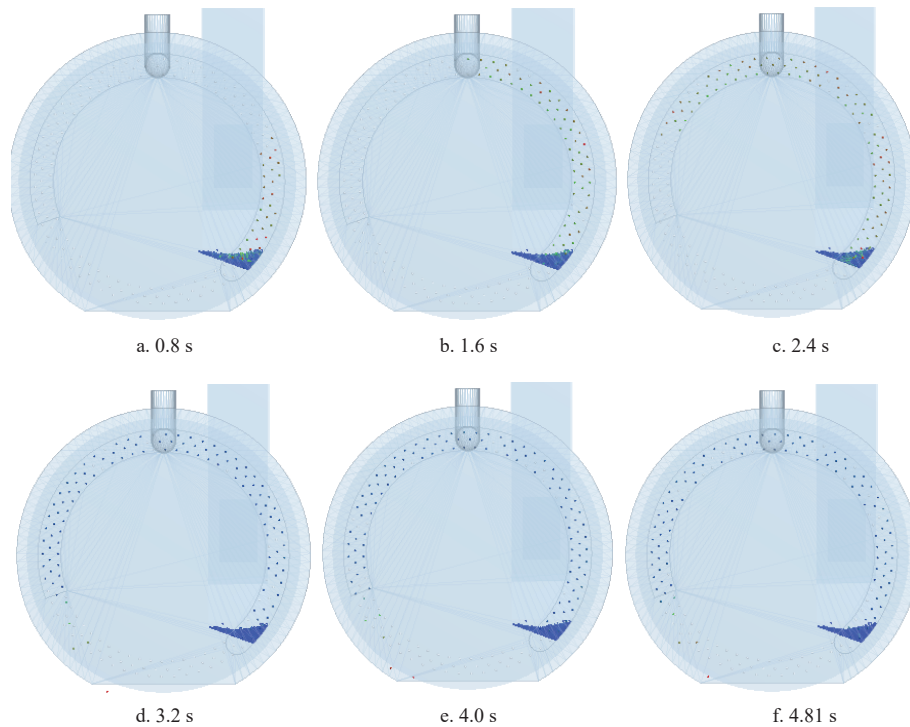
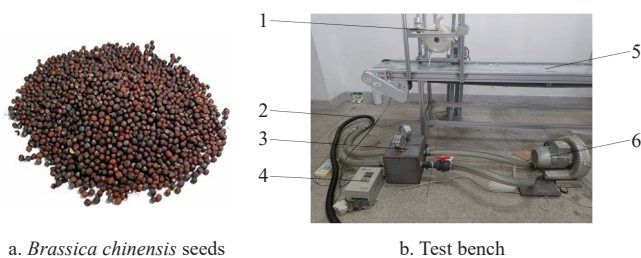


Figure 10 Coupling simulation process of metering device with a diameter of 0.8 mm (seed suction effect)

Table 2 Coupling simulation results

Hole diameter/mm	Position	Qualification rate/%	Miss seeding rate/%
0.8	Inner ring	80.59	19.41
	Middle ring	85.07	14.93
	Outer ring	77.61	22.39
1.0	Inner ring	91.04	8.96
	Middle ring	94.03	5.97
	Outer ring	92.54	7.46
1.2	Inner ring	97.01	2.99
	Middle ring	98.51	1.49
	Outer ring	97.01	2.99

“Shanghai Ai Ji”. A self-built test bench was utilized to study the seeding performance of a three-row air-suction *Brassica chinensis* precision metering device. The test equipment mainly consisted of a metering device, conveyor belt, variable frequency motor, vacuum tube, positive pressure tube, u-manometer, conveyor belt frequency modulator, wind pressure detection system, fan, and fan frequency regulator. The relative movement between the metering device and the conveyor belt was used to simulate the movement of the planter in the field. The velocity of the conveyor belt was changed by adjusting the frequency converter to simulate the different field driving states of the planter^[25] as shown in Figure 11.



a. *Brassica chinensis* seeds
 b. Test bench
 1. Metering device 2. Negative pressure tube 3. Wind pressure detection system
 4. Conveyor belt frequency modulator 5. Conveyor belt 6. Fan

Figure 11 Test materials and seeding performance test bench

2.5.2 Test methods and index

Considering the analysis of the previous experiment, the negative pressure, rotational speed of the seeding plate and diameter of the suction hole were chosen as experimental factors^[26,27]. From theoretical analysis, the critical minimum negative pressure required to adsorb one seed was calculated to be 0.342 kPa. Taking into account the pressure loss, the negative pressure range was determined to be 2.5-4.5 kPa. According to the pre-experiment, it was found that miss-seeding occurred seriously when the rotational speed exceeded 3 rad/s. When the rotational speed was less than 1 rad/s, it was difficult for the seeds to be adsorbed in the sucking holes due to the poor mobility of the seeds. For the determination of optimal rotational speed, rotational speed ranging from 1-3 rad/s was selected from the pre-experiment.

According to theoretical calculation, the diameter of the suction hole of the seeding plate was about 1.1 mm. The size of the suction pore was the main factor affecting the adsorption effect. Combined with the pre-experiment, the adjustable range of suction hole diameter was 0.8-1.2 mm. Three seeding plates with different diameters of suction holes were processed, the effects of the above three factors on the seeding performance were studied, and the optimal parameters combination was determined. Experiments using the Box-Behnken design were carried out, and the experimental design is listed in Table 3.

Table 3 Levels of experimental factors

Level	Factors		
	X_1 /kPa	X_2 /rad·s ⁻¹	X_3 /mm
-1	2.5	1	0.8
0	3.5	2	1.0
1	4.5	3	1.2

Note: X_1 is the negative pressure; X_2 is the rotational speed of the seeding plate; X_3 is the diameter of the suction hole.

The performance test of the metering device was duplicated three times under each group of data, and the mean was used as the experimental result. Going by Chinese national standard GB/T6973-

2005 Testing Methods of Single Seed (Precision Drills), the miss seeding rate and the qualification rate were selected as the evaluation rate^[28], and the calculation equations were as follows:

$$M = \frac{N_1}{N} \times 100\% \tag{8}$$

$$Q = \frac{N_2}{N} \times 100\% \tag{9}$$

where, M is the miss seeding rate, %; Q is the qualification rate, %; N_1 is the number of miss seeding; N_2 is the qualification number; N is the theoretical seeding numbers. The theoretical spacing was x (40-50 mm), and the distance between adjacent seeds on the conveyor belt was L . When $0.5x < L < 1.5x$, it was qualification, and where $L > 1.5x$ ^[29], it was miss seeding.

3 Results and discussion

3.1 Test results

The Box-Behnken design scheme was tested using Design-Expert 13.0 Software. The qualification rate and miss-seeding rate were considered as the performance index^[30]. The scheme and results are listed in Table 4.

Table 4 Experiment design and results

No.	Experimental factors			Results					
	X_1	X_2	X_3	$Q_1/\%$	$M_1/\%$	$Q_2/\%$	$M_2/\%$	$Q_3/\%$	$M_3/\%$
1	-1	-1	0	82.14	16.31	82.33	12.45	83.14	15.36
2	1	-1	0	87.42	11.91	91.26	5.65	85.63	6.12
3	-1	1	0	76.35	20.88	76.24	20.98	75.16	16.93
4	1	1	0	79.80	15.13	80.75	16.35	84.33	17.16
5	-1	0	-1	80.32	18.41	80.41	17.15	81.75	16.15
6	1	0	-1	84.24	11.83	83.54	12.45	84.83	12.67
7	-1	0	1	81.37	16.92	80.33	18.67	82.75	16.73
8	1	0	1	83.19	11.44	83.44	12.67	89.62	8.81
9	0	-1	-1	81.77	17.34	85.31	9.23	83.43	9.62
10	0	1	-1	80.13	16.92	80.19	15.62	80.37	17.92
11	0	-1	1	83.34	14.47	84.55	12.19	85.64	11.79
12	0	1	1	77.17	16.55	82.93	16.65	84.15	13.14
13	0	0	0	85.64	11.22	88.1	10.61	86.24	12.34
14	0	0	0	87.21	11.42	88.92	9.34	93.15	5.26
15	0	0	0	86.55	11.34	87.33	11.74	89.21	6.86
16	0	0	0	85.44	12.59	90.36	8.17	91.62	7.95
17	0	0	0	87.83	11.71	91.25	8.46	91.32	5.64

Note: Q_1 is the inner ring qualified index; M_1 is the inner ring missed seeding index; Q_2 is the middle ring qualified index; M_2 is the middle ring missed seeding index; Q_3 is the outer ring qualified ring index; M_3 is the outer ring missed seeding index.

It can be seen from Table 4 that the seeding performance of the inner ring was poor, probably due to the low height of the seed layer caused by the special slope structure of the seed filling chamber. The qualification rate and miss-seeding rate of the inner, middle, and outer rings were analyzed. By performing multiple regression fitting on the experimental results, the regression model of the qualification rate and miss-seeding rate were obtained.

3.2 Regression mathematical model

1) Establishment and significance test of the regression model of qualification rate

Through multiple regression fitting of the simulation test data, the regression model of the influence of the hole diameter, the rotational speed, and the negative pressure on the qualification rate of inner, middle, and outer rings were obtained as follows:

$$Q_1 = 86.53 + 1.81X_1 - 2.65X_2 - 0.1737X_3 - 0.4575X_1X_2 - 0.525X_1X_3 - 1.13X_2X_3 - 1.71X_1^2 - 3.39X_2^2 - 2.54X_3^2 \tag{10}$$

$$Q_2 = 89.19 + 2.46X_1 - 2.92X_2 - 0.225X_3 - 1.11X_1X_2 - 0.005X_1X_3 - 0.875X_2X_3 - 3.93X_1^2 - 2.62X_2^2 - 3.33X_3^2 \tag{11}$$

$$Q_3 = 90.31 + 2.70X_1 - 1.73X_2 + 1.47X_3 + 1.67X_1X_2 + 0.9475X_1X_3 + 0.3925X_2X_3 - 3.45X_1^2 - 4.79X_2^2 - 2.12X_3^2 \tag{12}$$

From the analysis of variance of the regression equation of the qualification rate of inner, middle, and outer rings in Tables 5-7, it can be seen that the F value of the regression model of the qualification rate was 15.46, 7.41, and 7.29 respectively, and the corresponding significance level $P < 0.01$ indicated that the fit of the three models was highly significant. The F value of misfit was 1.70, 2.48, and 0.15 respectively, and the corresponding significance level P was 0.3033, 0.2005, and 0.9259 respectively, so the effect was not significant, which showed that there are no other main factors affecting the qualification rate of inner, middle and outer rings regression equation. The coefficient of determination R^2 of the regression equation was 0.9521, 0.9050, and 0.9036 respectively, which indicated that the three models could accurately reflect the relationship between negative pressure, rotational speed, hole diameter, and qualification rate. As shown in Tables 5-7, for the interaction term (X_1X_2) of negative pressure and rotational speed, the interaction term of suction hole diameter and negative pressure

Table 5 Variance analysis of inner ring regression model

Performance index	Source	Sum of square	df	Mean square	F value	p value
Inner ring qualification rate	Model	187.10	9	20.79	15.46	0.0008**
	X_1	26.17	1	26.17	19.47	0.0031**
	X_2	56.29	1	56.29	41.86	0.0003**
	X_3	0.2415	1	0.2415	0.1796	0.0144*
	X_1X_2	0.8372	1	0.8372	0.6227	0.4559
	X_1X_3	1.10	1	1.10	0.8200	0.3953
	X_2X_3	5.13	1	5.13	3.82	0.0917
	X_1^2	12.38	1	12.38	9.21	0.0190*
	X_2^2	48.44	1	48.44	36.03	0.0005**
	X_3^2	27.15	1	27.15	20.20	0.0028**
Residual	9.41	7	1.34			
Lack of fit	5.28	3	1.76	1.70	0.3033	
Pure Error	4.13	4	1.03			
Cor Total	196.51	16				
Inner ring miss seeding rate	Model	141.90	9	15.77	16.71	0.0006**
	X_1	61.66	1	61.66	65.35	<0.0001**
	X_2	11.16	1	11.16	11.83	0.0108*
	X_3	3.28	1	3.28	3.47	0.0047**
	X_1X_2	0.4556	1	0.4556	0.4829	0.5095
	X_1X_3	0.3025	1	0.3025	0.3206	0.5889
	X_2X_3	1.56	1	1.56	1.66	0.2391
	X_1^2	7.85	1	7.85	8.32	0.0235*
	X_2^2	38.80	1	38.80	41.12	0.0004**
	X_3^2	11.16	1	11.16	11.83	0.0108*
Residual	6.61	7	0.9436			
Lack of fit	5.38	3	1.79	5.88	0.0600	
Pure Error	1.22	4	0.3052			
Cor Total	148.51	16				

Note: * represents significant difference ($0.01 < p < 0.05$); ** represents highly significant difference ($p < 0.01$).

(X_1X_3), and the interaction term of suction hole diameter and rotational speed (X_2X_3), the corresponding P values were all greater than 0.05 which showed that they had no significant effect on the inner rate qualification rate. For the middle ring, the insignificant term was added to the inner ring by X_3 . For the outer ring, the insignificant term was added to the inner circle by X_2 , X_3 , and X_3^2 .

Table 6 Variance analysis of middle ring regression model

Performance index	Source	Sum of square	df	Mean square	F value	P value
Middle ring qualification rate	Model	281.38	9	31.26	7.41	0.0075**
	X_1	48.41	1	48.41	11.47	0.0117*
	X_2	68.09	1	68.09	16.13	0.0051**
	X_3	0.4050	1	0.4050	0.0959	0.7658
	X_1X_2	4.88	1	4.88	1.16	0.3178
	X_1X_3	0.0001	1	0.0001	0.0000	0.9963
	X_2X_3	3.06	1	3.06	0.7255	0.4225
	X_1^2	65.06	1	65.06	15.41	0.0057**
	X_2^2	28.81	1	28.81	6.83	0.0348*
	X_3^2	46.72	1	46.72	11.07	0.0126*
Residual	29.55	7	4.22			
Lack of fit	19.22	3	6.41	2.48	0.2005	
Pure Error	10.33	4	2.58			
Cor Total	310.93	16				
Middle ring miss seeding rate	Model	259.83	9	28.87	10.94	0.0023**
	X_1	61.22	1	61.22	23.20	0.0019**
	X_2	113.10	1	113.10	42.87	0.0003**
	X_3	4.10	1	4.10	1.56	0.2524
	X_1X_2	1.18	1	1.18	0.4462	0.5256
	X_1X_3	0.4225	1	0.4225	0.1601	0.7010
	X_2X_3	0.9312	1	0.9312	0.3530	0.5711
	X_1^2	37.97	1	37.97	14.39	0.0068**
	X_2^2	5.97	1	5.97	2.26	0.1763
	X_3^2	27.77	1	27.77	10.52	0.0142*
Residual	18.47	7	0.9436			
Lack of fit	9.48	3	1.79	1.41	0.3639	
Pure Error	8.99	4	0.3052			
Cor Total	278.30	16				

Note: * represents significant difference ($0.01 < p < 0.05$); ** represents extremely significant difference ($p < 0.01$).

Table 7 Variance analysis of outer ring regression model

Performance index	Source	Sum of square	df	Mean square	F value	p value
Outer ring qualification rate	Model	297.70	9	33.08	7.29	0.0079**
	X_1	58.37	1	58.37	12.87	0.0089**
	X_2	23.91	1	23.91	5.27	0.0553
	X_3	17.35	1	17.35	3.83	0.0914
	X_1X_2	11.16	1	11.16	2.46	0.1608
	X_1X_3	3.59	1	3.59	0.7919	0.4031
	X_2X_3	0.6162	1	0.6162	0.1359	0.7233
	X_1^2	50.16	1	50.16	11.06	0.0127*
	X_2^2	96.67	1	96.67	21.32	0.0024**
	X_3^2	18.91	1	18.91	4.17	0.0805
Residual	31.74	7	4.53			
Lack of fit	3.17	3	1.06	0.1478	0.9259	
Pure Error	28.58	4	7.14			
Cor Total	329.45	16				
Outer ring miss seeding rate	Model	282.82	9	31.42	6.41	0.0114*
	X_1	52.07	1	52.07	10.62	0.0139*
	X_2	61.94	1	61.94	12.63	0.0093**
	X_3	4.34	1	4.34	0.8845	0.3783
	X_1X_2	22.42	1	22.42	4.57	0.0698
	X_1X_3	4.93	1	4.93	1.01	0.3494
	X_2X_3	12.08	1	12.08	2.46	0.1605
	X_1^2	48.03	1	48.03	9.80	0.0166*
	X_2^2	35.53	1	35.53	7.25	0.0310*
	X_3^2	28.52	1	28.52	5.82	0.0467*
Residual	34.32	7	4.90			
Lack of fit	1.87	3	0.6218	0.0766	0.9694	
Pure Error	32.45	4	8.11			
Cor Total	317.14	16				

Note: * represents significant difference ($0.01 < p < 0.05$), ** represents extremely significant difference ($p < 0.01$).

The normal plot of the residuals obtained after eliminating the insignificant factors is shown in Figure 12. It can be seen that the residual scatter of the inner ring qualification rate regression model was basically on a straight line, indicating that the three factors fit the qualification rate better. From the F -values of the regression model, it can be concluded that the factors influencing the inner ring qualification rate in the order of priority were rotational speed (X_2), negative pressure (X_1), and suction hole diameter (X_3) for the middle ring, it was $X_2 > X_1 > X_3$, for the outer ring, it was $X_2 > X_1 > X_3$. The regression model after excluding the insignificant factors was:

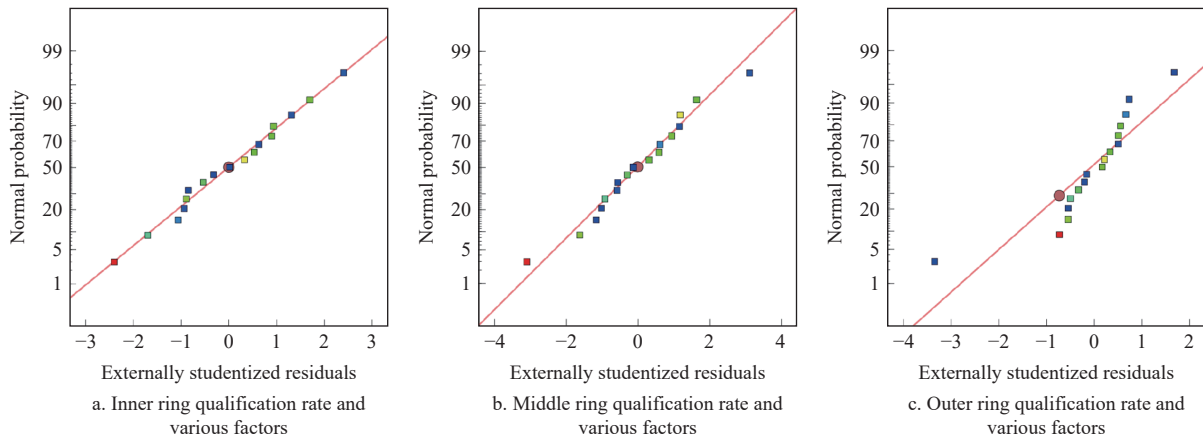


Figure 12 Fitting residual normal map

$$Q_1 = 86.53 + 1.81X_1 - 2.65X_2 - 0.1737X_3 - 1.71X_1^2 - 3.39X_2^2 - 2.54X_3^2 \quad (13)$$

$$Q_2 = 89.19 + 2.46X_1 - 2.92X_2 - 3.93X_1^2 - 2.62X_2^2 - 3.33X_3^2 \quad (14)$$

$$Q_3 = 90.31 + 2.70X_1 - 3.45X_1^2 - 4.79X_2^2 \quad (15)$$

2) Establishment and significance test of the regression model of miss seeding rate

The regression model for the effect of negative pressure, the rotational speed of the seeding plate, and hole diameter on the miss seeding rate of inner, middle, and outer rings were obtained by fitting multiple regressions to the simulated test data. The regression equations were as follows:

$$M_1 = 11.66 - 2.78X_1 + 1.18X_2 - 0.64X_3 - 0.3375X_1X_2 + 0.275X_1X_3 + 0.625X_2X_3 + 1.37X_1^2 + 3.04X_2^2 + 1.63X_3^2 \quad (16)$$

$$M_2 = 9.66 + 2.77X_1 + 3.76X_2 + 0.7163X_3 + 0.5425X_1X_2 - 0.325X_1X_3 - 0.4825X_2X_3 + 3.00X_1^2 + 1.19X_2^2 + 2.57X_3^2 \quad (17)$$

$$M_3 = 7.61 - 2.55X_1 + 2.78X_2 - 0.7363X_3 + 2.37X_1X_2 - 1.11X_1X_3 - 1.74X_2X_3 + 3.38X_1^2 + 2.90X_2^2 + 2.60X_3^2 \quad (18)$$

Based on the results in Tables 5-7, it can be seen that the *F*

value of the regression model of the miss-seeding rate was 16.71, 10.94, and 6.41 respectively, and the corresponding significance level $p < 0.05$ indicated that the fit of the three models was significant. The *F* value of misfit was 5.88, 1.41, and 0.08 respectively, and the corresponding significance level p was 0.06, 0.3639, and 0.9694 respectively, so the effect was not significant, which showed that there were no other main factors affecting the miss seeding rate of inner, middle and outer rings regression equation.

Figure 13 shows the normal graph of residuals obtained after excluding insignificant factors. It can be seen that the distribution of residual scatter points was close to a straight line, indicating that the fitting regression model of miss seeding rate to each factor was good. From the *F* value of the regression model, it can be concluded that the primary and secondary order of factors affecting the miss-seeding rate were X_2 , X_3 , and X_1 , for the middle ring, it was X_2 , X_1 , and X_3 , for the outer ring, it was X_2 , X_1 , and X_3 . The regression model after removing insignificant factors is:

$$M_1 = 11.66 - 2.78X_1 + 1.18X_2 - 0.64X_3 + 1.37X_1^2 + 3.04X_2^2 + 1.63X_3^2 \quad (19)$$

$$M_2 = 9.66 - 2.77X_1 + 3.76X_2 + 3.00X_1^2 + 2.57X_2^2 \quad (20)$$

$$M_3 = 7.61 - 2.55X_1 + 2.78X_2 + 3.38X_1^2 + 2.90X_2^2 + 2.60X_3^2 \quad (21)$$

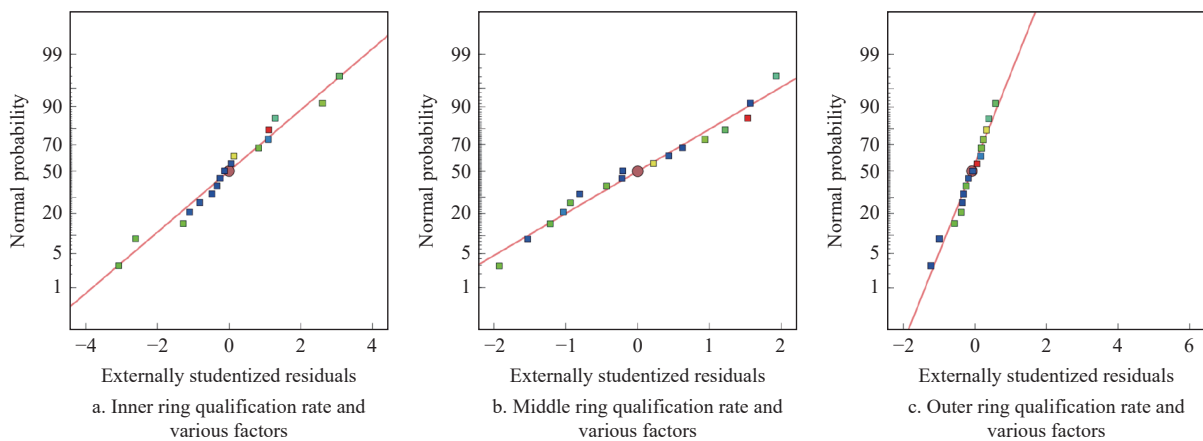


Figure 13 Fitting residual normal map

3.3 Interactive effects of different factors on performance index

3.3.1 Interactive effects of different factors on qualification rate

After processing the data with Design-Expert 13.0 Software, the effect of negative pressure, rotational speed, and hole diameter on the qualification rate was obtained and the interaction of the

factors was analyzed by means of a response surface. One of the factors was downscaled to a zero level^[31], and the effect of the interaction between the remaining two factors on the qualification rate of the inner, middle, and outer rings was plotted, as shown in Figures 14-16.

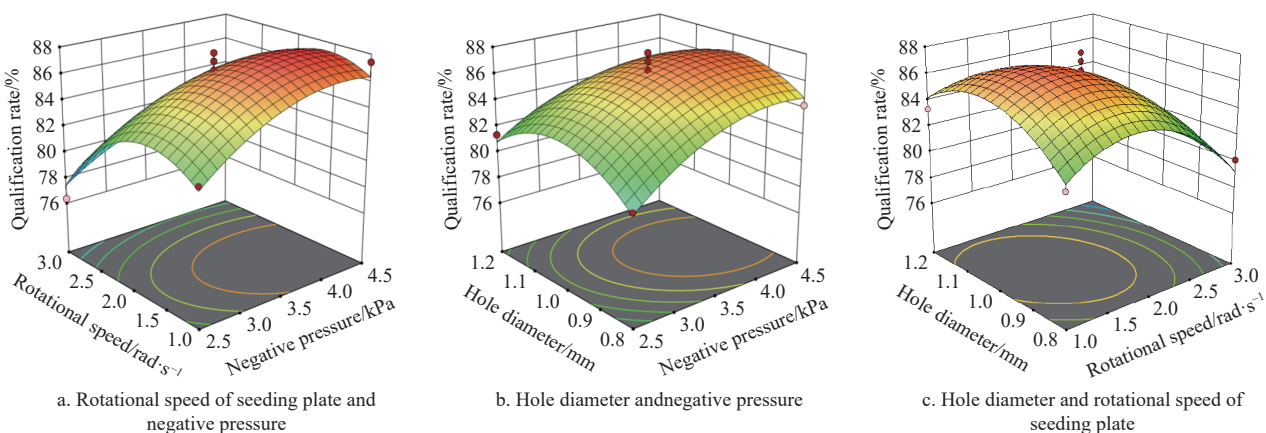


Figure 14 Effects of different factors on the inner ring qualification rate

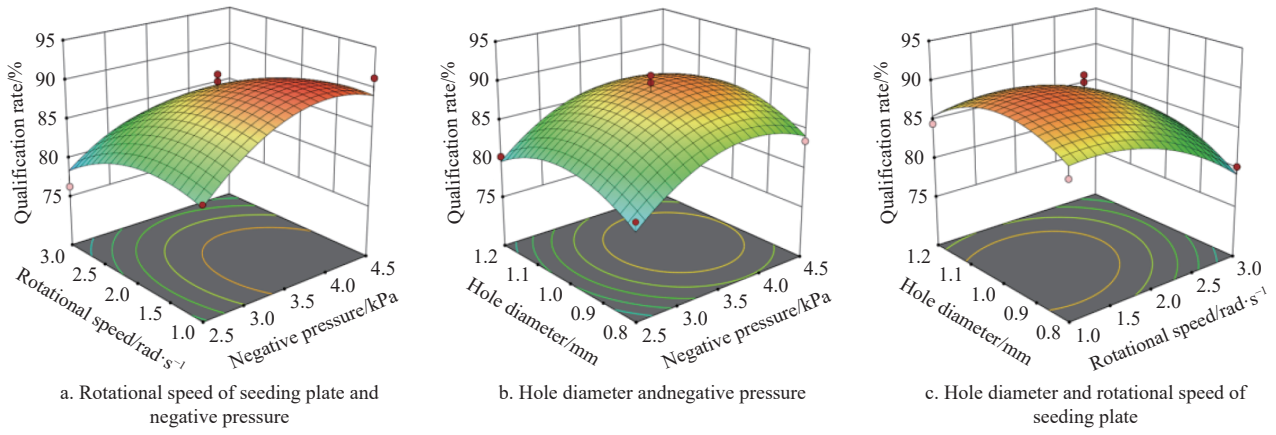


Figure 15 Effects of different factors on the middle ring qualification rate

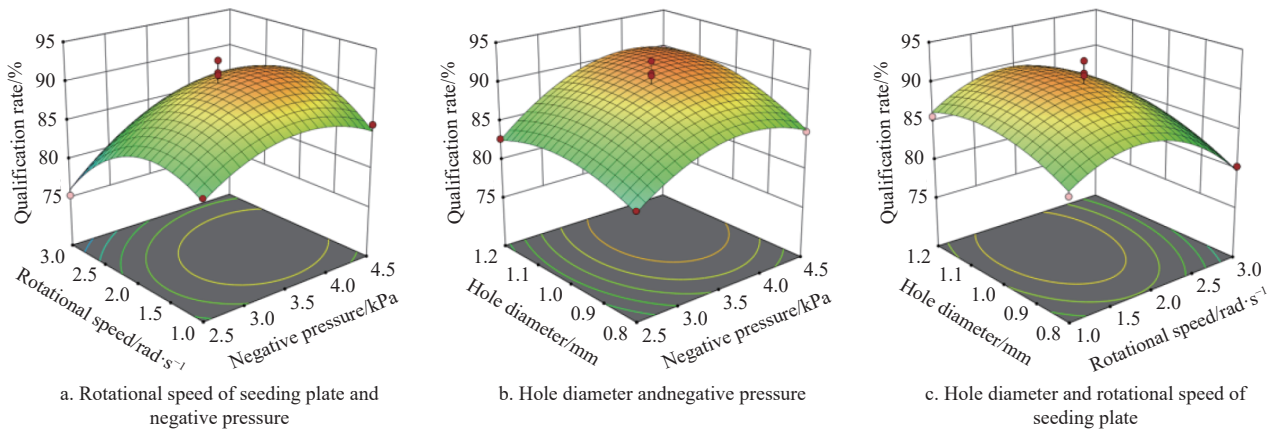


Figure 16 Effects of different factors on the outer ring qualification rate

The response surface diagram of the interaction of negative pressure and rotational speed on the inner ring qualification rate is shown in Figure 14a. It can be seen from Figure 14 that when the negative pressure was constant, the qualification rate first increased and then decreased with increase in the rotational speed. When the rotation speed was constant, the qualification rate first increased and then decreased with increase in negative pressure. The inner ring qualification rate was higher when the negative pressure was 3.2-4.5 kPa and the rotational speed was 1.0-2.2 rad/s. The response of the interaction of hole diameter and negative pressure on the inner ring qualification rate at a rotational speed of 2 rad/s is shown in Figure 14b. The qualification rate increased and then decreased as the negative pressure increased at a given rotational speed. At a certain negative pressure, as the diameter of the hole increased, the qualification rate tended to increase and then decrease. When the hole diameter was 0.85-1.12 mm and the negative pressure was 3.3-4.5 kPa, the inner ring qualification rate was higher. As shown in Figure 14c, when the hole diameter was constant, the qualification rate first increased and then decreased with increase in rotational speed. When the rotational speed was constant, the qualification rate first increased and then decreased with increase in the hole diameter. When the hole diameter was 0.87-1.14 mm and the rotational speed was 1.0-2.1 rad/s, the inner ring qualification rate was higher.

The response surface diagram of the interaction of negative pressure and rotational speed on the middle ring qualification rate is shown in Figure 15a. As can be seen from Figure 15a, the changing trend of middle ring qualification rate was consistent with that of inner ring qualification rate. When the negative pressure was 3.5-

4.0 Pa and the rotational speed was 1.7-2.2 rad/s, the qualification rate was relatively high. As shown in Figure 15b, when the negative pressure was 3.3-3.7 kPa and the hole diameter was 0.9-1.1 mm, the qualification rate was relatively high. Figure 15c shows that when the rotational speed was constant, the qualification rate first increased and then decreased with increase in the hole diameter. When the hole diameter was constant, the qualification rate decreased with increase in the rotational speed. It can be seen from Figure 16a and Figure 16b that the changing trend of outer ring qualification rate was consistent with that of the inner and middle rings. Figure 16c shows that the qualification rate was relatively high when the rotational speed was 1.5-2.0 rad/s and the hole diameter was 0.9-1.0 mm.

3.3.2 Interactive effects of different factors on miss seeding rate

The effect of the interaction between the remaining two factors on the miss-seeding rate of inner, middle, and outer rings was plotted, as shown in Figures 17-19.

The response surface of the interaction between negative pressure and rotational speed on the inner ring miss seeding rate at a hole diameter of 1.0 mm is shown in Figure 17a. The miss-seeding rate was lower when the negative pressure was between 3.4-4.5 kPa and the rotational speed was between 1.1-2.5 rad/s. As shown in Figure 17b, the miss-seeding rate was low when the hole diameter was 0.82-1.12 mm and the negative pressure was 3.5-4.5 kPa. The response surface plot of the interaction of hole diameter and rotational speed on the miss-seeding rate at a negative pressure of 3 kPa is shown in Figure 17c. The miss-seeding rate was lower when the hole diameter was 0.95-1.15 mm and the rotational speed was 1.2-2.2 rad/s.

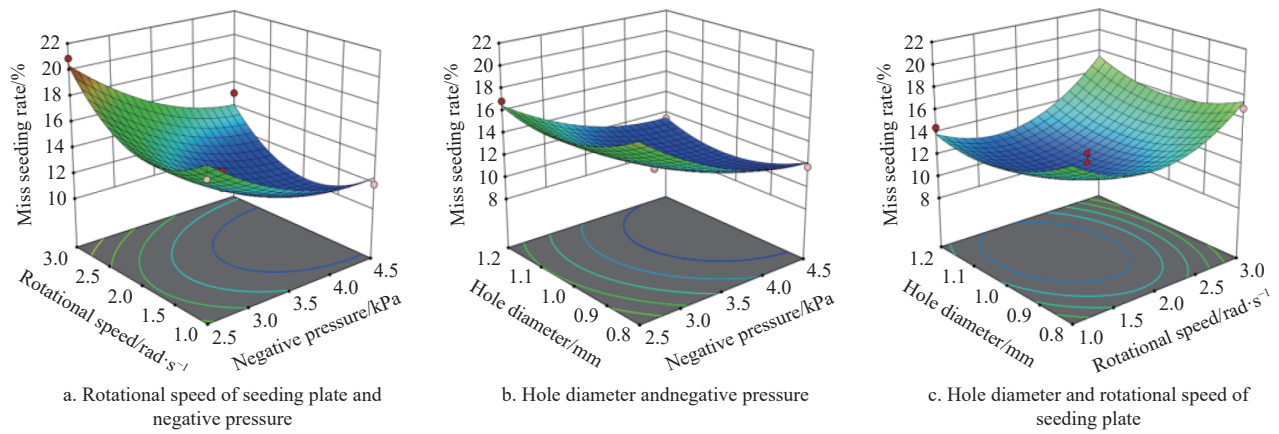


Figure 17 Effect of different factors on the inner ring miss seeding rate

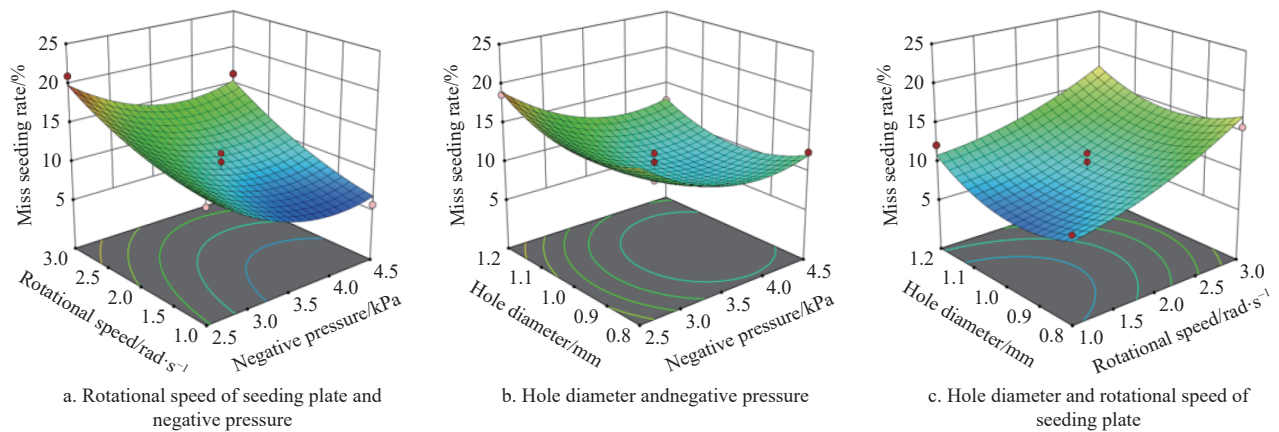


Figure 18 Effects of different factors on the middle ring miss seeding rate

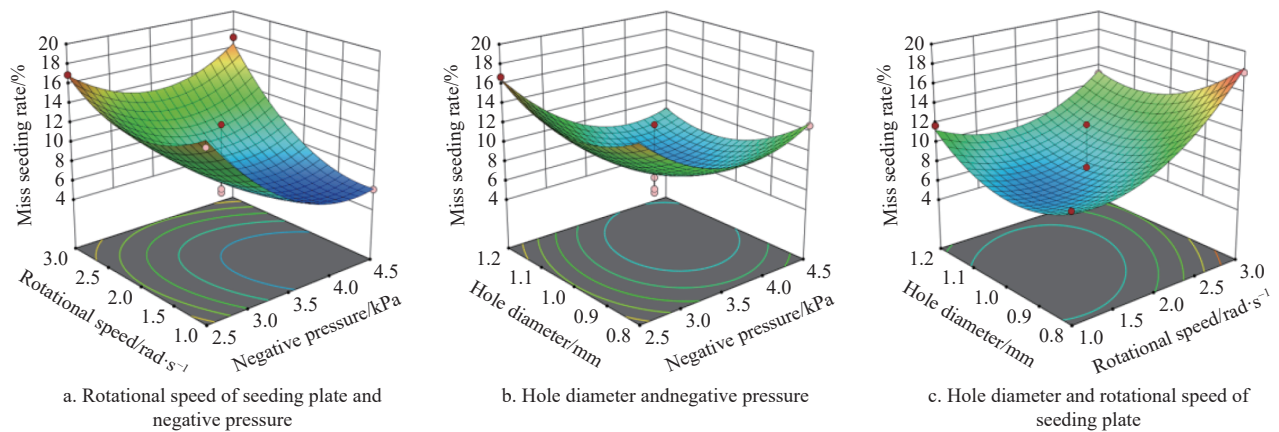


Figure 19 Effects of different factors on the outer ring miss seeding rate

Figure 18a shows that when negative pressure was constant, the middle ring miss-seeding rate decreased with an increase in the rotational speed. When the rotational speed was constant, the miss-seeding rate decreased with an increase in negative pressure. As can be seen from Figure 18b, the changing trend of the middle ring miss seeding rate was consistent with that of the inner ring. The miss-seeding rate was relatively low when the negative pressure was 3.7-4.1 kPa and the hole diameter was 0.9-1.0 mm. It can be seen from Figure 18c that when the rotational speed was constant, the miss-seeding rate first decreased and then increased with the increase of the hole diameter. When the hole diameter was constant, the miss-seeding rate increased with an increase in rotational speed. Figure 19a shows that the outer ring miss-seeding rate was relatively low when the negative pressure was 4.0-4.5 kPa and the rotational speed

was 1.0-1.5 rad/s. Figure 19b shows that the outer ring miss-seeding rate was relatively low when the negative pressure was 3.3-3.7 kPa and the hole diameter was 0.9-1.0 mm. Figure 19c shows that the outer ring miss-seeding rate was relatively low when the rotational speed was 1.0-1.5 rad/s and the hole diameter was 0.9-1.0 mm.

3.4 Parameters optimization

In order to obtain a better combination of parameters, the parameters were optimized. A parametric mathematical model was established and the regression equations for the qualification rate and miss-seeding rates were analyzed in combination with the boundary conditions for negative pressure, rotational speed, and hole diameter to obtain non-linear programming using the optimization module of Design-Expert 13.0 Software^[32,33]. The objective function and constraints are shown in Equation (19). The

best parameters were obtained as negative pressure of 3.96 kPa, a rotational speed of 1.49 rad/s, and a hole diameter of 1.1 mm, with a qualification rate of inner, middle, and outer rings of 87.580%, 90.548%, 90.117% respectively and a miss seeding rate of inner, middle and outer rings of 10.915%, 7.139%, and 5.920%, respectively.

$$\begin{cases} \min (M_1, M_2, M_3) \\ \max (Q_1, Q_2, Q_3) \\ \text{s.t.} \begin{cases} 2.5 \text{ kPa} \leq X_1 \leq 4.5 \text{ kPa} \\ 1 \text{ rad/s} \leq X_2 \leq 3 \text{ rad/s} \\ 0.8 \text{ mm} \leq X_3 \leq 1.2 \text{ mm} \end{cases} \end{cases} \quad (22)$$

3.5 Experimental verification

In an attempt to evaluate the seeding performance of the optimized metering device, the seeding performance tests were carried out using a self-built test bench with the parameters (negative pressure of 3.96 kPa, rotational speed of 1.49 rad/s, and hole diameter of 1.10 mm). The average values of five repeat tests were noted and compared with the optimized values, as listed in Table 8. It was demonstrated that the experimental verification results were similar to the optimized results under the optimum combination of parameters. The miss-seeding rate in the experimental verification results was larger than that in the optimized results, which was mainly caused by the vibration of the metering device and the sealing factor.

Table 8 Experimental verification results

Type	Position	Verification value
Qualification rate/%	Inner ring	85.59
	Middle ring	90.15
	Outer ring	91.22
Miss seeding rate/%	Inner ring	13.43
	Middle ring	7.46
	Outer ring	7.13

In order to make the experiment more realistic, as well as to further verify the seeding performance level of the optimized seed-metering device, field experiments on seeding performance were carried out at the Shanghai Academy of Agricultural Sciences on 16 April, 2022. The test machine and test scenario are shown in Figure 20, while Figure 21 shows the distance between seeds measured in the field, and the test parameters are consistent with the bench experiment. The results showed that the qualification rate in the field trial results was slightly lower than the bench experiment



Figure 20 Test machine and scenario

results and the optimized results under the optimal combination of parameters, which was mainly due to the unevenness of the real land, resulting in a larger vibration amplitude of the seed-metering device and seeds not being easily adsorbed.



Figure 21 Measuring the distance between seeds

4 Conclusions

In this study, a CFD-DEM coupling method to simulate the effects of negative pressure, rotational speed of seeding plate, and suction hole diameter on the seeding performance of the metering device was designed. The CFD-DEM coupling model accurately observed the phenomenon of miss-seeding in the metering device, and the following conclusions were drawn:

1) A three-row air-suction *Brassica chinensis* precision metering device was optimized to improve the low seeding performance of previous seed metering devices using the principle of negative pressure seed suction and positive pressure seed cleaning. The diameter range of the suction holes on the seeding plate was determined by measuring the triaxial dimensions of *Brassica chinensis* seeds to be 1.07-1.10 mm.

2) The effects of different numbers of suction holes and different shapes of suction holes on the airflow field were analyzed using ANSYS 17.0 Software. It was observed that when the number of suction holes was 60 and the shape of the suction holes was conical, it was beneficial to the stability of the flow field and easy to fill the seed. The effect of different suction hole diameters on the seeding effect was analyzed by CFD-DEM coupling simulation, and it was found that the seeding performance was poorer when the suction hole diameters were 0.8 mm. The outer ring suction holes on the seed plate had a poor seed-filling effect by pre-experiment and coupling simulation analysis, so the following analysis was mainly based on the outer ring suction effect.

3) The self-made metering device test bench was used to optimize the parameters of the metering device by using three factors and three levels according to Box-Behnken experimental design method. The best parameters were obtained as negative pressure of 3.96 kPa, rotational speed of 1.49 rad/s, and hole diameter of 1.10 mm, with qualification rates of inner, middle, and outer rings as 87.58%, 90.548%, and 90.117%, respectively, and miss seeding rate of inner, middle and outer rings as 10.915%, 7.139%, and 5.92% respectively, which was better than the national standard. The experimental verification results were similar to the optimized results under the optimum combination of parameters.

Acknowledgements

This research was financially supported by the National Key

R&D Program of China “Vegetable Intelligent Fine Production Technology and Equipment R&D” (Grant No. 2017YFD0701302).

[References]

- [1] Tang Y, Wang L M, Xie Y D, Yu X N, Lin L J, Li H, et al. Effects of intercropping accumulator plants and applying their straw on the growth and cadmium accumulation of *Brassica chinensis* L. *Environ Sci Pollut Res Int*, 2020; 27(31): 39094–39104.
- [2] Cao J S, Yu X L, Ye W Z, Lu G, Xiang X. Functional analysis of a novel male fertility CYP86MF gene in Chinese cabbage (*Brassica campestris* L. ssp. *chinensis* makino). *Plant Cell Rep*, 2006; 24(12): 715–723.
- [3] Ma J, Li M Y, Wang F, Tang J, Xiong A S. Genome-wide analysis of DoF family transcription factors and their responses to abiotic stresses in Chinese cabbage. *BMC Genomics*, 2015; 16(9): 1–14.
- [4] Yang L, Yan B X, Yu Y M, He X T, Liu Q W, Liang Z J, et al. Global overview of research progress and development of precision maize planters. *Int J Agric & Biol Eng*, 2016; 9(1): 9–26.
- [5] Yuan Y M, Ma X, Jin H X, Yin H Y. Study on vacuum chamber fluid field of air suction seed—metering device for rice bud—sowing. *Transactions of the CSAM*, 2005; 36(6): 42–45. (in Chinese)
- [6] Yatskul A, Lemiere J P, Cointault F. Influence of the divider head functioning conditions and geometry on the seed's distribution accuracy of the air-seeder. *Biosyst Eng*, 2017; 161: 120–134.
- [7] Amit R, Bikash M, Ravindra B. Experimental modeling and simulation of supercritical fluid extraction of *Moringa oleifera* seed oil by carbon dioxide. *Chem Eng Commun*, 2017; 204(8): 957–964.
- [8] Ren B, Zhong W Q, Chen Y, Chen X, Jin B S, Yuan Z L, et al. CFD-DEM simulation of spouting of corn-shaped particles. *Particuology*, 2012; 10(5): 562–572.
- [9] Tong Z B, Zheng B, Yang R Y, Yu A B, Chan H K. CFD-DEM investigation of the dispersion mechanisms in commercial dry powder inhalers. *Powder Technol*, 2013; 240: 19–24.
- [10] Jerzy R, Aleksander Z, Nikhil M, Szymon N. The discrete element method with deformable particles. *Int J Numer Meth Engng*, 2018; 114(8): 828–860.
- [11] Zubov A, Wilson J F, Kroupa M, Soos M, Kosek J. Numerical modeling of viscoelasticity in particle suspensions using the discrete element method. *Langmuir*, 2019; 35(39): 12754–12764.
- [12] Liu D Y, Song J L, Ma J L, Chen X P, Berend V W. Gas flow distribution and solid dynamics in a thin rectangular pressurized fluidized bed using CFD-DEM simulation. *Powder Technol*, 2020; 373: 369–383.
- [13] Taghinezhad J, Jafari A, Alimardani R. Development and evaluation of a new mechanism for sugarcane metering device using analytical hierarchy method and response surface methodology. *Sugar Tech*, 2015; 17(3): 258–265.
- [14] Lei X L, Liao Y T, Liao Q X. Simulation of seed motion in seed feeding device with DEM-CFD coupling approach for rapeseed and wheat. *Comput Elect Agri*, 2016; 131: 29–39.
- [15] Han D D, Zhang D X, Jing H R, Yang L, Cui T, Ding Y Q, et al. DEM-CFD coupling simulation and optimization of an inside-filling air-blowing maize precision seed-metering device. *Comput Elect Agri*, 2018; 150: 426–438.
- [16] Lai Q H, Sun K, Yu Q X, Qin W. Design and experiment of a six-row air-blowing centralized precision seed-metering device for *Panax notoginseng*. *Int J Agric Biol Eng*, 2020; 13(2): 111–122.
- [17] Zhang K X, Sun Y Y, Liu L, Liu X X, Zhao X Y. Design and test of variable diameter pneumatic drum type bean seed metering device. *INMATEH-Agric Eng*, 2020; 60(1): 9–18.
- [18] Chinese Academy of Agricultural Mechanization Sciences. *Agricultural machinery design manual-Volume 1*. Beijing: China Agricultural Science Press, 2007; 1885p. (in Chinese)
- [19] Zhai J B, Xia J F, Y Z. Design and experiment of pneumatic precision hill-drop drilling seed metering device for hybrid rice. *Transactions of the CSAM*, 2016; 47(1): 75–82.
- [20] Xu S Y. Design of pneumatic precision seed metering device for carrot. 2020; 42(12): 46-51. (in Chinese)
- [21] Li B H. Design and motion process simulation of a double-row precision seed metering device. Nanjing Tech University, 2021. (in Chinese)
- [22] Yin W Q, Zhao L, Li H, Hu F, Yu H M. Design and experiment on suction nozzle type hole of pneumatic-sheave combined vegetable precision metering device. *Transactions of the CSAM*, 2019; 50(4): 68–77. (in Chinese)
- [23] Fallak S S, Sverker P E. Vacuum nozzle design for seed metering. *Transactions of the ASAE*, 1984; 23(51): 688–696.
- [24] Hu H J, Zhou Z L, Wu W C, Yang W H, Li T, Chang C, et al. Distribution characteristics and parameter optimisation of an air-assisted centralised seed-metering device for rapeseed using a CFD-DEM coupled simulation. *Biosyst Eng*, 2021; 208: 246–259.
- [25] Xue P, Xia X Y, Gao P Y, Ren D, Hao Y J, Zheng Z Q, et al. Double-setting seed-metering device for precision planting of soybean at high speeds. *Transactions of the ASABE*, 2019; 62(1): 187–196.
- [26] Zahra A, Saman A M. Real time laboratory and field monitoring of the effect of the operational parameters on seed falling speed and trajectory of pneumatic planter. *Comput Elect Agri*, 2018; 145: 187–198.
- [27] Xing H, Wang Z M, Luo X W, He S Y, Zang Y. Mechanism modeling and experimental analysis of seed throwing with rice pneumatic seed metering device with adjustable seeding rate. *Comput Elect Agri*, 2020; 178: 1–16.
- [28] Jin X, Li Q W, Zhao K X, Zhao B, He Z T, Qiu Z M. Development and test of an electric precision seeder for small-size vegetable seeds. *Int J Agric Biol Eng*, 2019; 12(2): 75–81.
- [29] Li Z D, Yang W C, Wu Y Y, He S, Wang W W, Chen L Q. Performance analysis and experiments of seed filling assisted by groove-tooth of pneumatic disc precision metering device for rapeseed. *Transactions of the CSAE*, 2020; 36: 57–66. (in Chinese)
- [30] Sun X P, Li H, Qi X D, Nyambura S M, Yin J Q, Ma Y L, et al. Performance parameters optimization of a three-row pneumatic precision metering device for brassica chinensis. *Agronomy*, 2022; 12(5): 1011–1026.
- [31] Wu K, Chen J, Lou J, Yu Y, Li J. Design and Parameters Optimization of pteris vittata automatic sowing machine for phytoremediation. *Int J Eng*, 2020; 33: 694–701.
- [32] Shi L R, Sun B G, Zhao W Y, Yang X P, Xin S L, Wang J X. Optimization and test of performance parameters of elastic air suction type corn roller seed-metering device. *Transactions of the CSAM*, 2019; 50(10): 88–96. (in Chinese)
- [33] Wang Y Y, Li J D, Wang D W, Sun Q W, Yang W. Orthogonal experiment optimization on air-suction precision seed-metering device. *Transactions of the CSAM*, 2012; 43(S1): 54–59. (in Chinese)